ME 538: Advanced Fluid Mechanics
Computer Project

Presentable 23
Tech n problem 24
results 23
discussion 24
94/100

(Graduate Student)

December 9, 2016

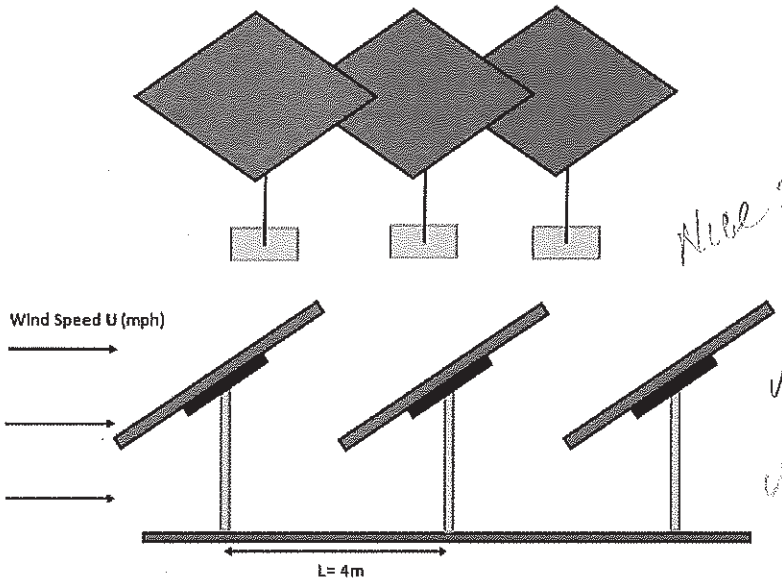

Nice study & report!
I would like
understand to see
a 3D and of
wakes to

Introduction/Background Information

In Hawaii, over 75% of the fuel used to create electricity must be imported culminating notoriously high energy costs [1]. With the highest energy rates in the country, and an abundance of sun year-round, Hawaii has quickly become the ideal market for solar energy. As a result, solar farms are quickly beginning to develop across the islands. At the end of the year, Eurus Energy will be beginning production on a 27.6 megawatt solar plant in Waianae, Hawaii. The solar plant, spanning 198 acres, will use photovoltaic panels produced by Canadian Solar, and racking system by Exosun [2].

The objective of this project is to model the flow of air around photovoltaic (PV) panels in a solar farm. Modeling the airflow around the panels will allow streamlines to be observed and the forces acting on the panels to be calculated. It is important to understand the forces acting on the panels so that the PV panels can be safely and appropriately mounted to the ground. Several variables must be considered in order to gain a comprehensive understanding of the flow scenarios the panels may encounter, including the angle of the panel relative to the ground, the speed of the wind, and the effects surrounding panels may have on the flow field of a single panel.

Approach/Description of Analysis

Within the scope of this project, the panel dimensions and circumstances of the installation were based on that of a solar farm intended to be built in Waianae, Hawaii. Each panel is mounted on the ground via a single axis track. The single axis track limits the rotation of the panels to +/- 50° in one dimension. The angles of the PV panels may change throughout the day in order to maximize exposure to the sun. Two potential angle cases will be considered, +50°, and -50°. These angles were chosen to specifically examine the extreme cases where the effects of the panels on the air flow are predicted to be the most pronounced.

In order to keep the flow of air in the model laminar, the flow speed was calculated to keep the reynolds number below 300,000, which is the critical reynolds number for flow over a flat plate. The characteristic linear dimension, D, used in Equation 1 to solve for the critical velocity, was assumed to be the vertical length along the angled plate seen by the incoming velocity as shown in Figure 1. The density and dynamic viscosity of air used are shown in Table 1. The resulting critical velocity was calculated to be roughly 6.16 m/s. Thus the inlet velocity adopted in the model to insure the flow would remain laminar was 4 m/s.

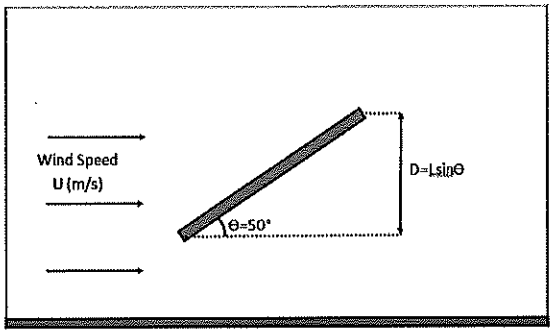

Figure 1. Characteristic Dimension, D.

[Eqn. 1]

$$Re = \frac{\rho U d}{\mu} \rightarrow U = \frac{Re\,\mu}{\rho d}$$

$$U = \frac{300{,}000\ (1.85508e{-}05\ Pa{\cdot}s)}{(1.18415\ kg/m^3)(0.996m)(sin\theta)}$$

$$U_{critical} = 6.15976\ \frac{m}{s}$$

Table 1. Material Properties of Air

Density (ρ)	1.18415 kg/m^3
Dynamic Viscosity (μ)	1.85508e-05 Pa-s

Each angle case was simulated with the same constant wind speed in the x-direction and three panels. In solar farms, the many rows of panels that are aligned may cause the flow over each row to vary. Thus, two additional cases, with 1 and 2 panels respectively, were analyzed at an angle of 50° and the established laminar wind speed, in order to understand the effects a single panel may have on the flow of air around adjacent panels. Therefore, four different cases as shown below in Figure 2, were analyzed.

Table 2. Cases Modeled in STAR-CCM+

Case	Angle of Panel (θ)	Number of Panels
A	+50°	1
B	+50°	2
C	+50°	3
D	-50°	3

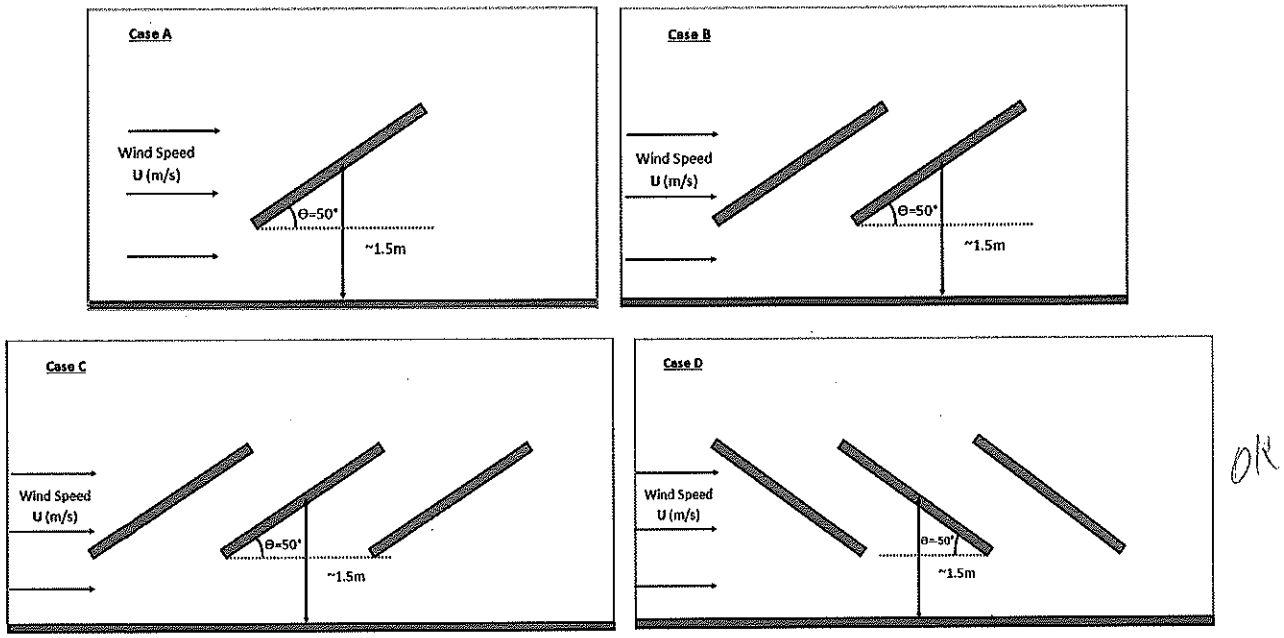

Figure 2. Various Cases Analyzed in STAR- CCM+ (Drawing Not to Scale)

Computational Domain

The computational domain was assumed to range from -5 to +10 in the x-direction and from -1 to +3 in the y-direction. This domain was chosen to allow for space in the domain to observe how the velocity flow is affected above the panel as well as after it passes the panels in the x-direction. As previously mentioned, the dimensions of the panels were based on a product from Canadian Solar, the module provider for the Eurus Energy project, and the circumstances surrounding the installation of the panels relative to the ground were based on the rack system of Exosun. Therefore, the panels were modeled to have a height of 996mm, depth of 8.5mm, width of 1972 mm, and a single axis track approximately 1.5m above the ground [3]. The width of the panels were irrelevant since the model of the flow was restricted to 2-dimensions. As a result, the width of the panel in z-direction, as modeled in STAR-CCM+, was set to 1 meter. Similarly, the distance between each panel was predetermined by the practices of Exosun and therefore modeled to be 4m. It should be noted that for the purposes of this project, the geometry of the panels were simplified to include solely the angled plate. The mounting system and the true width of the panels were neglected for the sake of time and computing resources.

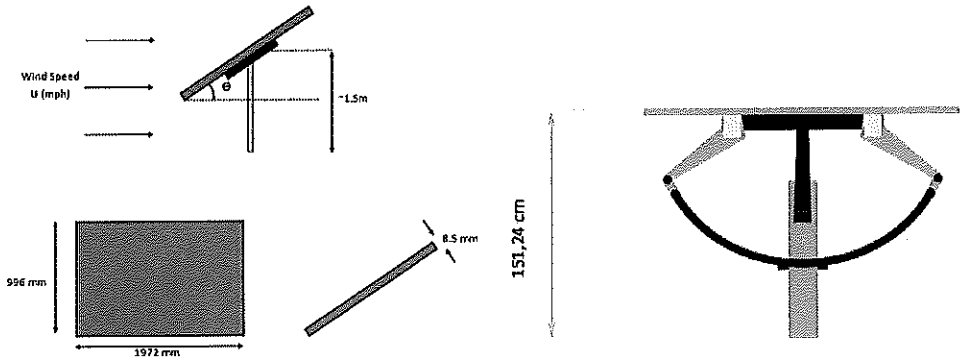

Figure 3. Canadian Solar 315 W Panel Dimensions [2] and Exosun Single-Axis Tracker [3]

Boundary Conditions

The inlet of the computational domain was considered to be a velocity inlet and the outlet was assumed to be a pressure outlet. In order to consider the effects the ground may have on the flow around the PV panel, the bottom of the computational domain was set to have a no-slip boundary condition. Similarly, in order to ignore the effects that the top face of the computational domain may have on the flow, and to simulate open air above the PV panels, a free-slip boundary condition was set at the top face of the domain. The remaining faces within the computation domain, including the front and back faces, as well as all faces of each panel, were also set to have no-slip boundary conditions.

Case Simulation and Analysis

Each case was individually simulated on STAR-CCM+. For all cases, the base size was set to 1e-02 m, the number of prism layers set to 5, and the surface growth rate set to 1.05 in order to create a mesh that was especially detailed near the panel and ground surfaces and efficiently but not overly dense elsewhere. Once the computational domain, initial and boundary conditions, and incoming flow velocity were established, the physical parameters of the flow were set. The incoming flow was initially modeled to be a steady, segregated, laminar flow of air with constant density. The simulation for each case was run for approximately 2000 iterations with the given parameters. It was observed that the velocity, pressure, drag and lift forces all exhibited oscillatory behavior. Therefore, the flow was altered to be modeled as an implicit unsteady flow and run for roughly 150,000 additional iterations or until the

observed characteristics stabilized. While the flow was being modeled as unsteady, the time step and the maximum inner iterations were varied to find an optimal balance between accuracy and time required. The appropriate time step was determined by multiplying the time step by the velocity of the inlet flow in order to approximate the distance traveled by a particle of fluid for each time step. The distance traveled by a fluid particle for each time step was then compared to the thickness of the PV panel. In order to insure that a fluid particle would not completely bypass the thickness of the plate in a single time step, the time step was set to 0.002 seconds. The maximum number of inner iterations was increased from 5 to 20 in attempt to lower the residuals. Increasing the inner iterations lowered residuals by nearly 99.5% from 0.80 down to 0.0045. While it is ideal to have residual values as small as possible, the time required to run a simulation with that level of accuracy was not worth the gain in precision. Therefore, after incrementally decreasing the maximum number of inner iterations and monitoring the residuals, the number of inner iterations was set to 10. OK

For each case, the velocity profile, pressure distribution, and streamlines were observed. Reports for the drag and lift forces on each panel were also created, along with plots of the drag and lift forces and coefficients against time.

Equations Solved

While simulating each case, STAR-CCM+ uses the material properties of the fluid, initial physical conditions including velocity at the inlet, and the given boundary conditions such as pressure outlet, no-slip, or free slip shear stress specifications to solve the Navier-Stokes equations. The residuals of the x- and y- momentum, and the continuity equation can be monitored to ensure that the equations are satisfied. This allows for the motion of the fluid to be accurately modeled. For all cases A through D, the drag and lift forces were plotted as functions of time for each panel. Due to the oscillatory nature of the flow, the forces exhibited a range of values as time progressed. Average maximum and minimum values for the drag and lift forces were taken from the STAR-CCM+ plots and used to solve for the drag and lift coefficients using Equations 2 and 3 shown below. The characteristic length, D, was calculated using the method shown in Figure 1, and found to be

OK

[Eqn. 2] $$C_d = \frac{2F_{drag}}{\rho U^2 D}$$

[Eqn. 3] $$C_L = \frac{2F_{lift}}{\rho U^2 D}$$

usually Δt is recorded as $\Delta t < \frac{\Delta x}{u}$ control volume $u \cdot \Delta x$ u - max velocity

Results

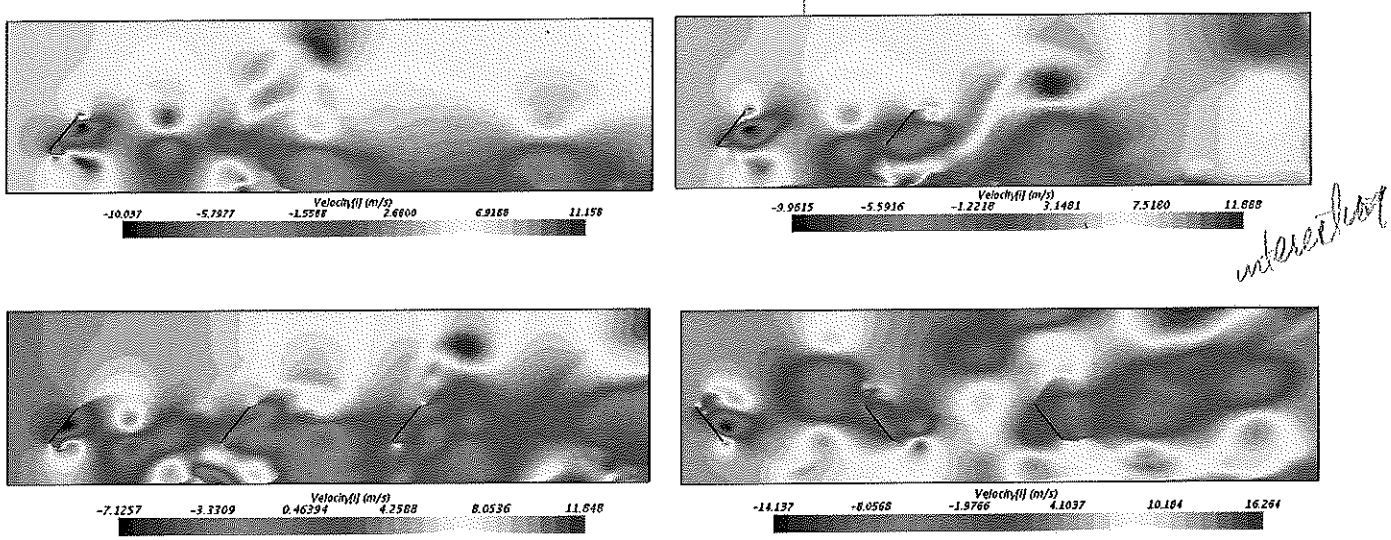

Figure 4. Velocity Profiles (Top: Case A and Case B, Bottom: Case C and Case D from left to right)

It can be observed from Figure 4 that as the air flows past a single angled panel, relatively high velocity eddies are created near the top and bottom edges of the panel. As a result, recirculation zones are also created behind the panel. Macroscopically, it can also be observed in cases A,B, and C, that the velocity in the upper half of the computational domain is 2 to 3 times higher than the velocity near the ground. Cases A through C contain an increasing number of PV panels. The comparison between these three cases allows the effect of a single PV panel on adjacent panels to be shown. It can be observed that as the air flows past the first panel on the left, the high velocity eddies are created. These eddies appear to alternate spawning at the top and bottom edges of each PV panel and cause the flow to have oscillatory behavior. The high velocity eddies spawning at the bottom edge of the left panel tend to flow up between the left and center panels. Similarly, the eddy formed at the bottom edge of the center panel flows up and between the center and right panel at a relatively high velocity before dispersing above all the panels. The recirculating eddies formed at the back of the panel also have relatively high velocity as compared to the inlet velocity of the air. However, the magnitude of velocity of these recirculating eddies behind the left panel in each case tends to decrease as the number of panels increases. The recirculating eddy flows down towards the ground below the next panel, likely being pushed down by the high velocity eddy formed above it.

The three panels in case C are angled at +50° and the panels in case D are angled at -50°. Comparing these two case at the extreme ends of the range of rotation of the panel allow the effect of changing the angle to be observed. The same patterns of eddy formation at the ends and back of the panels occur in both cases. However, the most notable difference appears to be that the high velocity eddies formed at the bottom of the panels no longer seem to flow up between the panels. Instead the eddies propagate in the +x-direction underneath the panels. As a result the high velocity eddies form a cup-like formation around the following panel lifting it up. Lastly, the magnitude of the velocities achieved in case D are significantly higher than those reached in the previous three cases.

Streamlines

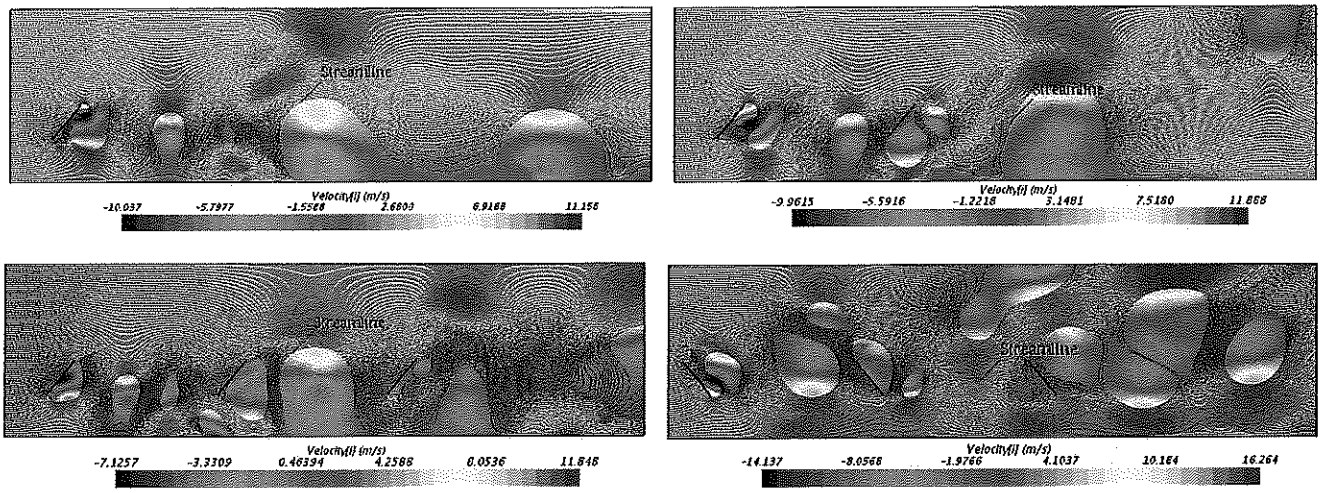

Figure 5. Velocity Streamlines (Top: Case A and Case B, Bottom: Case C and Case D from left to right)

The streamlines shown for each case in Figure 5 clearly display the high velocity eddies previously discussed. The fluid particles entering on the left, flow past the first panel on the left and form eddies near the top and bottom edges of the left panel. The eddies seen in case A propagate to the right, unobstructed, and disperse. However, in cases B through D, those eddies can no longer simply flow to the right. Instead they must navigate around the next panels. As the number of panels increases the streamlines become increasingly complex. Similarly, with the angle change in case D, the pathways the fluid particles follow, particularly in the bottom half of the domain, agree with the convoluted velocity profile in Figure 4. The streamlines show the eddies coming off the bottom edges splitting and cupping around the following panel. The voids in the streamline display also coincide with the low pressure pockets shown in Figure 6. The streamlines, velocity profile, and pressure distribution all agree in that the high velocity recirculation zones can easily be observed to coincide with the voids in the streamlines and the low pressure pockets satisfying the momentum balance in the x-direction.

Pressure Distribution

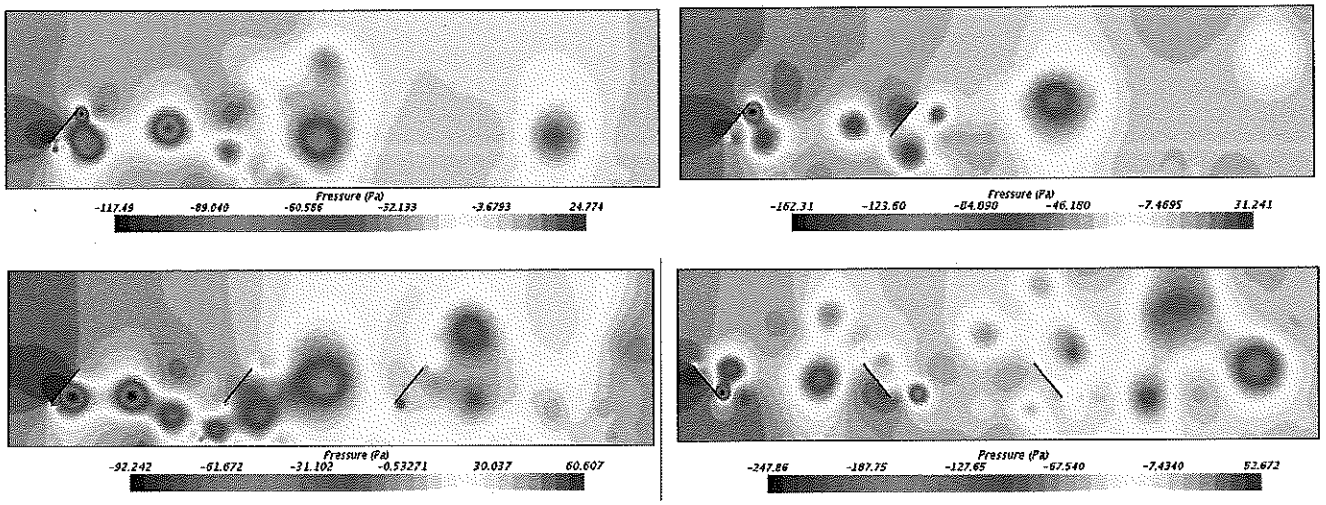

Figure 6. Pressure Distribution (Top: Case A and Case B, Bottom: Case C and Case D from left to right)

The overarching trend in all cases, appears to be that the pressure near the inlet is initially high and begins to lower as the flow propagates to the right. The pressure distribution plots shown in Figure 6, are consistent with the velocity profiles shown in Figure 4. The eddies of very low pressure relative to the outlet of the computational domain coincide with regions of high velocity, conserving momentum and satisfying the continuity equation. In a fashion very similar to that of the velocity profiles, the pressure distribution plots of each case show eddies of very low pressure forming at the top and bottom edges of the PV panels. These eddies also alternate and flow between the panels. It should also be noted that high pressures are developed at the inlet face of each panel. The highest pressure occurs at the inlet facing surface of the left panel. The high pressure regions at the inlet facing surfaces of each panel are slightly lower than the high pressure achieved on the panel before it. Therefore, it can be seen in cases C and D that the pressure exerted on the left panels are higher than the pressures exerted on the center and right panels. The pressure experienced at the left panel also increases significantly as the number of panels in the domain increases, ranging from 24.777 Pa in case A, 31.241 Pa in case B, 60.607 Pa in case C, and 52.672 Pa in Case D. This range of maximum pressures suggests that the pressure distribution is more dominantly affected by adjacent panels rather than the angle of the panel.

Drag Force and Coefficient

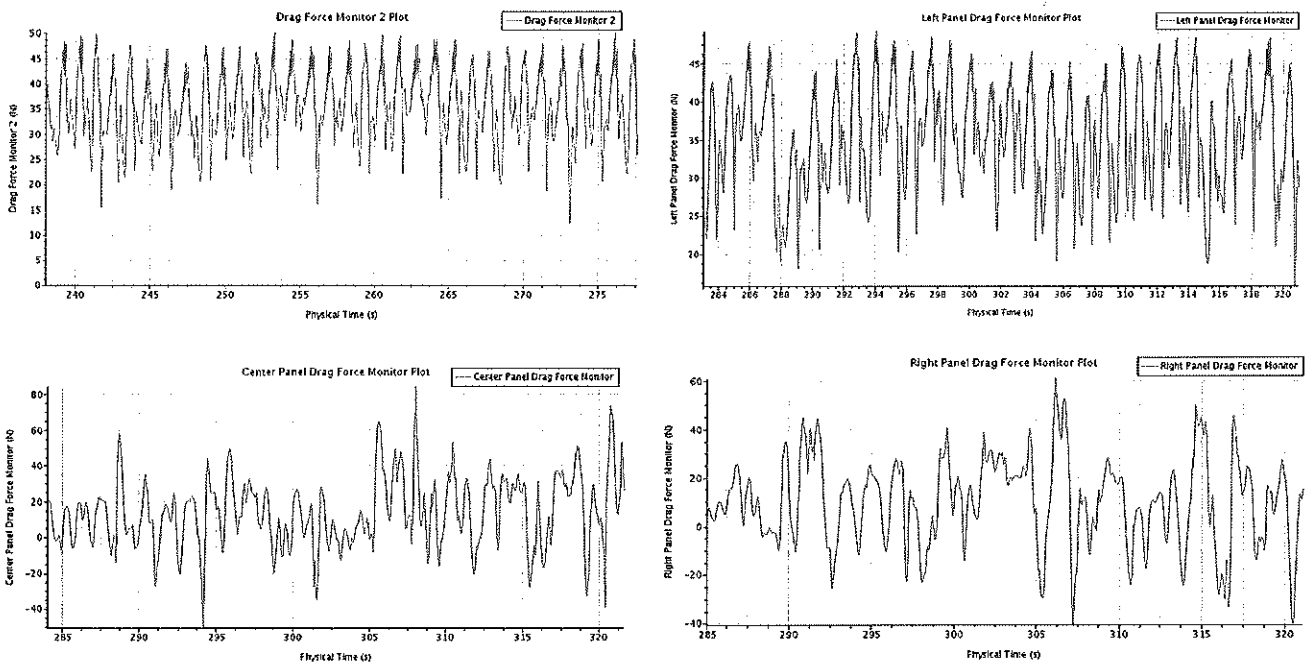

Figure 7. Drag Force Plots (Top Left: Case A Left Panel) (Top Right: Case C Left Panel) (Bottom Row: Case C Center, and Right Panels Respectively)

Reports and plots of the drag forces as functions of time were monitored for each panel in all cases. In the interest of conserving space, the plots of the drag forces as functions of time shown in Figure 7 are limited to cases A and C. In some aspects, the drag forces on each panel were relatively similar. The drag forces on all panels exhibited oscillatory, and semi-periodic behavior. The plots began to differ as panels were added in cases B,C, and D. In the latter cases, the drag forces became increasingly chaotic. In case A, the drag forces on the left panel ranged between 15 to 50 N. When the

center panel was added in case B, the range of drag forces acting on the left panel narrowed slightly by about 14%. When the right panel was added in case C the range of drag forces acting on the left panel narrowed even further by 2% from the drag experienced in case B. Similarly from case B to C, the range of drag forces acting on the center panel narrowed by about 9%. Perhaps the biggest difference between the drag forces exerted on the center panel in cases B and C is that the minimum forces were generally negative, indicating that the drag forces were now pushing the panel in the negative x-direction. The right panel exhibited the most chaotic behavior. The negative drag forces experienced by the right panel in case C were nearly equal in magnitude to the drag forces in the positive x-direction. In case D, while many of the drag force minimums were negative, there were also a noticeable amount of minimums that were acting in the positive x-direction. This deviates from case C, where nearly all the minimum drag forces exerted on the right panel were negative. This indicates that when the angle of the panel relative to the ground is positive, the force exerted on the right panel in the x-direction oscillate between pushing in the positive and negative directions. When the angle of the panel is negative relative to the ground, the force exerted by the fluid in the x-direction is more likely to be in the positive direction rather than the negative direction.

Overall, it may be observed from the values in Table 2, that the drag force exerted on the left panel increases as the number of panels following it increases. Similarly, the drag force exerted on the left panel is always the highest with respect to the panels that follow it. The panel on the right experiences the lowest drag force. Lastly, when the angle of the panel relative to the ground is negative, the drag force exerted on a panel is significantly higher than the drag force exerted when the angle of the panel is positive relative to the ground.

The range in drag forces experienced by each panel resulted in a corresponding drag coefficient range as shown in Table 2. The average drag forces and drag coefficients calculated by STAR-CCM+ nicely agree with the ranges of coefficients calculated using Equation 2.

Table 2. Results of Drag Force and Coefficient Range

Case	Panel	Drag Force Maximum (N)	Drag Force Minimum (N)	(STAR-CCM+) Net Drag Force	Drag Coeff. Maximum	Drag Coeff. Minimum	(STAR-CCM+) Drag Coeff
A	Left	49.6495	15.0300	29.469420461500768	6.8692	2.0795	4.064847861019607
B	Left	48.5976	18.9441	35.900013262933285	6.7236	2.6210	4.951848045775187
B	Center	73.7865	-23.4254	29.967286821989276	10.2086	-3.2410	4.133520776157154
C	Left	47.6888	18.5616	39.98347585769949	6.5979	2.5681	5.515098151611971
C	Center	54.7137	-33.9226	25.649282505100075	7.5698	-4.6944	3.5379192903963226
C	Right	38.9255	-25.0083	18.20341070855134	5.3855	-3.4600	2.5108771710859794
D	Left	84.7373	33.2786	50.89322223831048	11.7237	4.5904	7.019927854572291
D	Center	59.5220	5.1789	38.03435733613113	8.2351	0.7165	5.2462475895990055
D	Right	80.5128	-10.367	22.31737058044994	11.1392	-1.4370	3.078333901612939

Lift Force and Coefficient

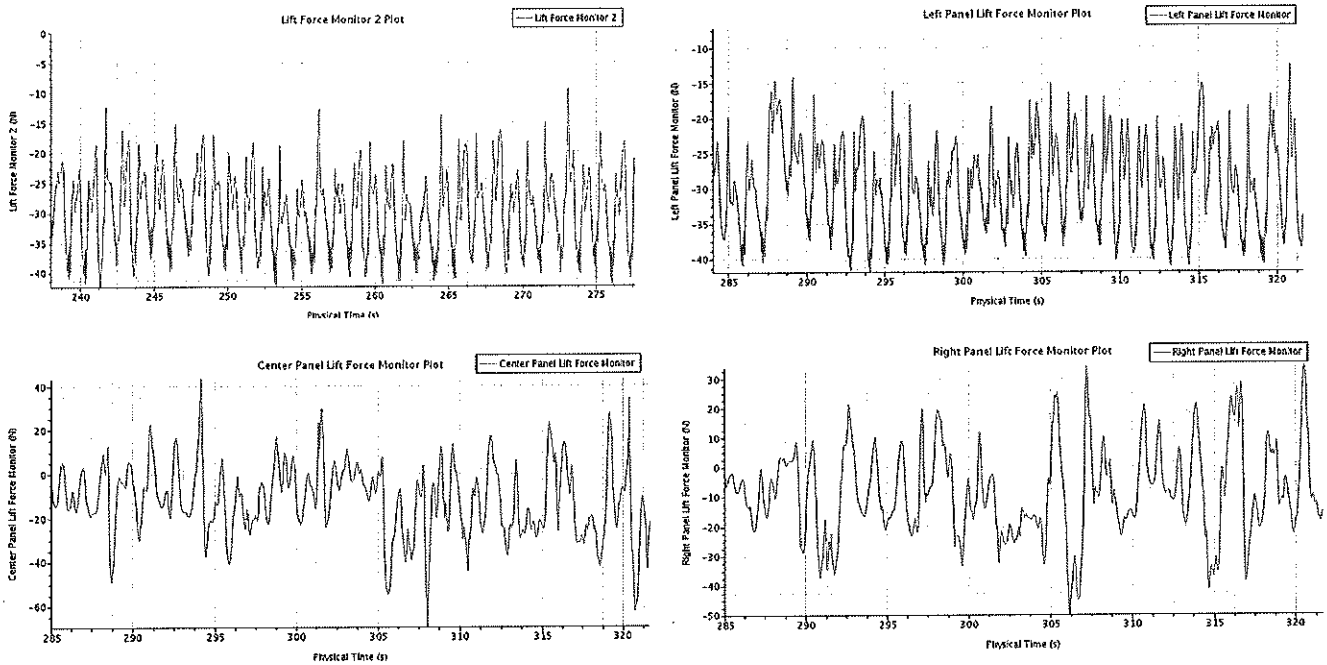

Figure 8. Drag Force Plots (Top Left: Case A Left Panel) (Top Right: Case C Left Panel) (Bottom Row: Case C Center, and Right Panels Respectively)

As with the drag forces, reports and plots of the lift forces as functions of time were monitored for each panel in all cases. In the interest of conserving space, the plots of the lifting forces as a function of time shown in Figure 7 are limited to case C. The lift forces exerted on the panels also showed oscillatory and semi-periodic behavior. It can be seen from both Figure 8, and the values in Table 3, that while the oscillating lifting forces acting on the left panels always remained negative, the forces acting on the center, and right panels oscillated between positive and negative lift forces. Therefore the forces acting on the left panel, in the y-direction, in cases A through C always pushed the panel down towards the ground. Contrastly, the forces acting on the center and right panels in the y-direction varied between pushing the panel down and lifting it up. In regards to the average lift forces calculated in STAR-CCM+ shown in Table 3, several trends can be observed. First, as the number of panels increases, the lift force exerted on the first panel increases. Secondly, the magnitude of the force exerted in the y-direction on each panel in cases C and D decreased as the number of panels before it increased. That is to say, the lift force acting on the right panel is lower than the force acting on the center panel, and the force acting on the center panel is lower than the force acting on the first panel on the left. Lastly, when the angle of the panel relative to the ground is negative, the force acting in the y-direction generally tends to acts in the positive direction to lift the panel, while the force acting on the panels with the positive angle, acts in the negative direction, pushing the panels down. The magnitude of the forces acting on the panels in case D were also slightly higher than the forces acting on the respective panels in case C.

Table 3. Results of Lift Force and Coefficient Range

Case	Panel	Lift Force Maximum (N)	Lift Force Minimum (N)	(STAR-CCM+) Net Lift Force (N)	Lift Coeff. Maximum	Lift Coeff. Minimum	(STAR-CCM+) Lift Coeff
A	Left	-41.6684	-13.0688	-23.643041711236087	-5.7650	-1.8081	-3.261189600028567
B	Left	-41.2856	-14.8302	-28.91587592820034	-5.7120	-2.0518	-3.988495008573633
B	Center	23.3631	-62.3745	-25.518587354642012	3.2324	-8.6297	-3.5198919286611594
C	Left	-39.8321	-17.7211	-33.895060630038195	-5.5109	-2.4518	-4.675296037162861
C	Center	29.9598	-43.6533	-22.33539890659236	3.0382	-6.0396	-3.0808206285933193
C	Right	21.4513	-33.8332	-15.209269861425224	2.9679	-4.6809	5.515098151611971
D	Left	67.2322	26.4722	40.601518086947884	9.3018	3.6625	5.600347457307078
D	Center	47.3951	4.7416	32.221258484790766	6.5573	0.6560	4.444421083962897
D	Right	58.3023	-6.8400	18.414308279976648	8.0663	-0.9463	2.5476830535160877

Conclusion

In conclusion, arranging photovoltaic panels can be beneficial in the mitigation of drag and lift forces felt by the panels. This particular arrangement of the panels has shown to help reduce the drag and lift forces exerted on inner rows of panels. However, this arrangement of panels also causes an increases in the forces exerted on the first row of panels that the airflow encounters. This behavior should be considered during the installation of the panels to ensure that the outer rows of panels in a solar farm are appropriately mounted to be able to withstand higher forces without failing.

Modeling the cases of the extreme ends of the range of motion of the panel allow the forces to be estimated at what would intuitively be assumed to be the two positions that the maximum forces would occur. As the panels rotate throughout the day to follow the sun, the drag and lift forces exerted on the panels will vary. When the angle of the panel relative to the ground is negative, the drag and lift forces exerted on the panels will be higher than when the angle of the panel relative to the ground is positive. The changes in forces exerted on the panel can be attributed to the streamlines that high velocity eddies follow as the air flows past each panel.

A key parameter that would be worth further exploring in future models is the distance between each row of panels. It may be well worth the time to determine the optimal distance between each row of panels that would minimize the drag and lift forces exerted on the succeeding row of panels.

References:

[1] Gerdes, J. (2013, July 26). Why Hawaii Just Became An Even Better Market For Solar. Retrieved December 4, 2016, from http://www.forbes.com/sites/justingerdes/2013/07/26/why-hawaii-just-became-an-even-better-market-for-solar/#10d2ce72398a

[2] Wesoff, E. (2016, March 9). Vital Stats on the Biggest Solar Project in Hawaii. Retrieved November, 2016, from https://www.greentechmedia.com/articles/read/Vital-Stats-on-the-Biggest-Solar-Project-in-Hawaii

[3] DOUBLE-GLASS MODULE DYMOND CS6X-315|320|325|330P-FG. (2016, November). Retrieved November, 2016, from http://www.canadiansolar.com/fileadmin/user_upload/downloads/datasheets/v5.53/Canadian_Solar-Datasheet-Dymond-CS6X-P-FG-v5.53en.pdf

(Panel and Racking System Providers)
http://www.canadiansolar.com/solar-panels/dymond.html
http://www.exosun.net/solar-tracker-exotrack-hz/single-axis-tracker

Example of CFD of Panel:
http://www.iawe.org/Proceedings/11ACWE/11ACWE-Shademan.pdf